

Article

Synthesis and Characterization of Pd/La₂O₃/ZnO Catalyst for Complete Oxidation of Methane, Propane and Butane

Ralitsa Velinova ¹, Nina Kaneva ^{2,*}, Georgi Ivanov ¹, Daniela Kovacheva ¹, Ivanka Spassova ¹, Silviya Todorova ³, Genoveva Atanasova ¹ and Anton Naydenov ^{1,*}

¹ Institute of General and Inorganic Chemistry, Bulgarian Academy of Sciences, Acad. G. Bonchev St., Bldg. 11, 1113 Sofia, Bulgaria; raligeorgieva@svr.igic.bas.bg (R.V.); geoivnov@yahoo.com (G.I.); didka@svr.igic.bas.bg (D.K.); ispassova@svr.igic.bas.bg (I.S.); genoveva@svr.igic.bas.bg (G.A.)

² Laboratory of Nanoparticle Science and Technology, Department of General and Inorganic Chemistry, Faculty of Chemistry and Pharmacy, University of Sofia, 1164 Sofia, Bulgaria

³ Institute of Catalysis, Bulgarian Academy of Sciences, Acad. G. Bonchev St., Bldg. 11, 1113 Sofia, Bulgaria; todorova@ic.bas.bg

* Correspondence: nina_k@abv.bg (N.K.); naydenov@svr.igic.bas.bg (A.N.)

Abstract: The catalytic oxidation of volatile organic compounds (VOCs) is the subject of considerable interest due to its applications in environmental protection. Noble metal-based catalysts are widely employed to remove toxic compounds from gas mixtures. The objective of the present study was the synthesis of a palladium-containing catalyst deposited on a support modified with La₂O₃ zinc oxide. The composite support was initially obtained by a simple method, and then palladium was deposited on it by impregnation. Various methods, including N₂-physisorption, XRD, HRTEM, XPS, TPD, TPR, and FTIR, were used to characterize the material. The obtained catalyst was studied in the reaction of the complete oxidation of butane, propane, and methane. It was found that the addition of La₂O₃ to ZnO led to an improved pore texture. The catalytic tests showed that the reaction of the complete oxidation of butane on Pd/La₂O₃/ZnO proceeded at the lowest temperatures.

Keywords: Pd/La₂O₃/ZnO catalyst; methane; propane; butane



Academic Editors: Antonino Gulino, Tobias Krämer and Geun-Ho Han

Received: 14 November 2024

Revised: 30 December 2024

Accepted: 7 January 2025

Published: 9 January 2025

Citation: Velinova, R.; Kaneva, N.; Ivanov, G.; Kovacheva, D.; Spassova, I.; Todorova, S.; Atanasova, G.; Naydenov, A. Synthesis and Characterization of Pd/La₂O₃/ZnO Catalyst for Complete Oxidation of Methane, Propane and Butane. *Inorganics* **2025**, *13*, 17. <https://doi.org/10.3390/inorganics13010017>

Copyright: © 2025 by the authors. Licensee MDPI, Basel, Switzerland. This article is an open access article distributed under the terms and conditions of the Creative Commons Attribution (CC BY) license (<https://creativecommons.org/licenses/by/4.0/>).

1. Introduction

The degradation of organic pollutants from air and wastewater has been attempted in recent years using semiconductor photocatalysts (TiO₂, ZnO, CdS, WO₃, and others) because of their advantages, which include a low cost, high activity, and ease of scaling up [1–3]. As a common and stable semiconductor photocatalyst, zinc oxide is prone to photo-corrosion [4], has a large surface area, and is non-toxic [5,6]. Since oxygen vacancy and/or metal excess act as donor states that provide conduction electrons, this material is an n-type semiconductor. Since platinum and palladium are well-known active catalysts that increase the sensitivity against reducing gases, they are typically added in small amounts to ZnO, which is rarely used as a single phase for a gas sensor, to modify its gas-sensing properties [7]. It is thought that chemisorption is aided by the catalyst layer. Furthermore, the quick recombination of the electron–hole pair in ZnO, which restricts the catalytic degradation process, is one of its drawbacks. There have been numerous attempts to enhance ZnO's catalytic capabilities [8,9]. ZnO's optical, electrical, and magnetic characteristics are altered when it is doped with rare earth ions. The creation of nanomaterials based on trivalent rare earth ion-doped wide-bandgap semiconductors is, therefore, a focus of much research due to their special uses, which include, but are not limited to,

optoelectronic, electronic, spintronic, photocatalytic, and antibacterial applications. Based on the electronic transitions that take place within 4f energy shells, rare earth metals are currently being used as dopants for a variety of applications due to their properties of being highly conductive, magnetic, electrochemical, and luminescent [10–13]. Because of their high thermal stability and ability to capture photoinduced electrons, rare earth metals can lessen electron–hole pair recombination [14]. Rare earth elements' high surface basicity, rapid oxygen ion mobility, and strongly catalytic nature make them attractive options to improve gas oxidation applications [15]. Khatamian et al. [16] synthesized ZnO nanoparticles doped with Ln (La, Nd, or Sm) and found that the doped nanoparticles degraded PNP more quickly than pure ZnO. In comparison to pure ZnO, Ahmad et al. [17] found that the zinc oxide photocatalyst doped with three weight percent cerium had four times the catalytic efficiency. The use of semiconductor nanomaterials modified with rare earth metal oxides, like ZnO, in a catalytic process is, therefore, a promising strategy.

This work aimed to study a new lanthanum oxide-modified ZnO support and investigate the effects on the morphology, structure, and catalytic properties of a Pd catalyst based on it. Methane, propane, and butane oxidation were selected as the catalytic reactions for the tests because they are representative of the gases released by internal combustion engines that run on liquefied petroleum gas (LPG).

2. Results and Discussion

2.1. Catalytic Tests

The reaction of the complete oxidation of methane, propane, and butane was examined to assess the applicability of the synthesized Pd/La₂O₃/ZnO material as a catalyst for combustion. The results from the catalytic experiments are presented in Figure 1.

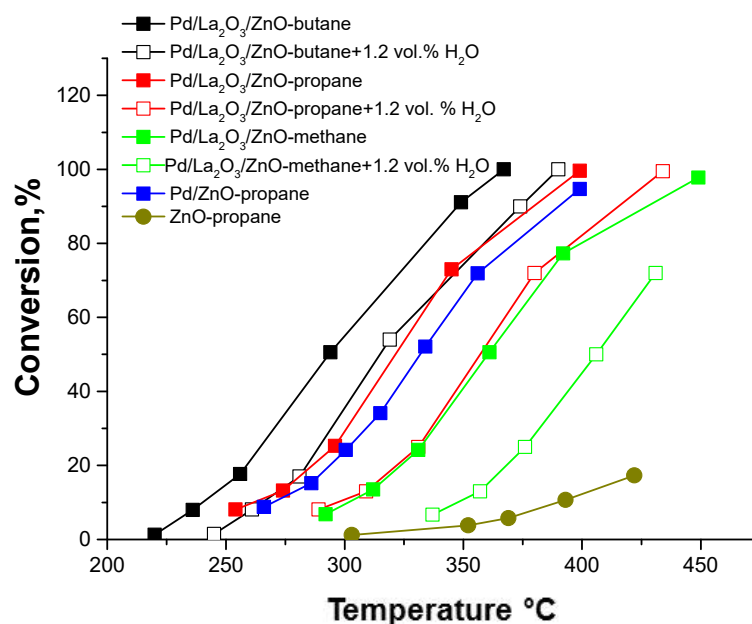


Figure 1. Temperature dependence of the conversion degree in the reactions of complete methane, propane, and butane oxidation and effect of water vapor.

As expected, the oxidation of methane showed the highest conversion temperature, and a decrease in reaction temperature from methane to butane was observed in correlation with the strength of the weakest H-C bond [18,19]. It was found that the catalyst Pd/La₂O₃/ZnO possessed high activity in the complete oxidation of methane, propane, and butane. The highest activity was registered towards butane with T₅₀ = 294 °C. For a more detailed study, propane was chosen due to its medium reactivity when compared

with butane and methane. Data on the catalytic activity in the reaction of the complete oxidation of propane for the ZnO support and Pd/ZnO catalyst in dry gas are also included for the sake of comparison. It was evident that the activity of the pure ZnO support was low, and the catalyst prepared with 2 mol.% La_2O_3 had higher activity ($T_{50} = 320\text{ }^\circ\text{C}$) compared to the catalyst without La_2O_3 ($T_{50} = 330\text{ }^\circ\text{C}$) in propane combustion. The water vapor (concentration of 1.2 vol.%) had a reversible, inhibitory effect, which was expressed as a shift in the S-curves to higher temperatures by about 25–45 $^\circ\text{C}$ (from butane to methane). The duration of the tests in the presence of water was fixed to 60 h, and the observed reaction order was approximately -0.1 . For isothermal operation, the construction of the catalytic reactor permits compensation for the adiabatic rise up to 80 $^\circ\text{C}$; thus, the catalyst bed temperature was kept constant (the deviations did not exceed $\pm 1\text{ }^\circ\text{C}$).

A number of techniques were used to characterize the catalysts prepared in order to evaluate the observed differences in their activity.

2.2. Nitrogen Physisorption

The results regarding the adsorption–desorption isotherms, pore size distributions, and texture parameters of the pure ZnO, $\text{La}_2\text{O}_3/\text{ZnO}$, and Pd/ $\text{La}_2\text{O}_3/\text{ZnO}$ fresh catalysts are shown in Figure 2 and in Table 1. According to the IUPAC classification, the adsorption–desorption isotherms for all studied samples were of type II with H3 hysteresis loops [20]. Type H3 is often associated with the slit pores formed between plate-like particles [21].

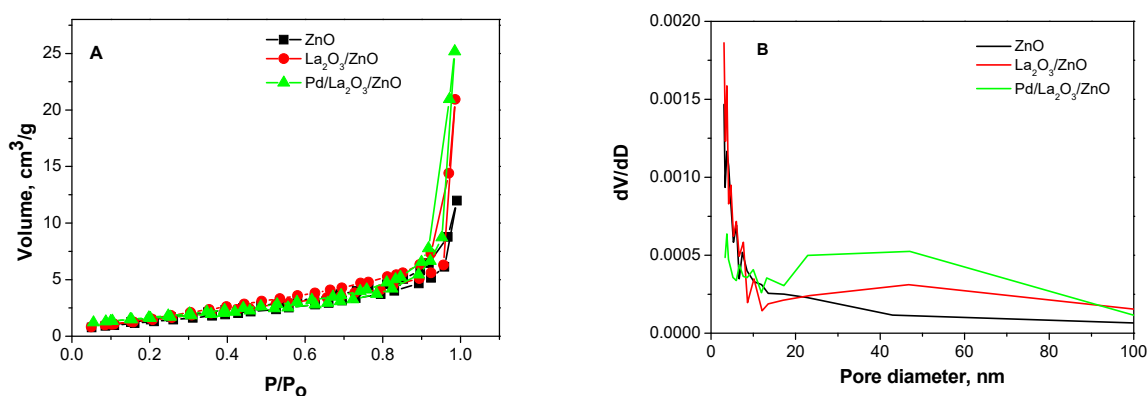


Figure 2. Adsorption–desorption isotherms (A) and pore size distributions (B) of pure ZnO, $\text{La}_2\text{O}_3/\text{ZnO}$, and Pd/ $\text{La}_2\text{O}_3/\text{ZnO}$ fresh catalysts.

Table 1. Specific surface areas (S_{BET}), total pore volumes (V_t), and average pore diameters (D_{av}) of pure ZnO, $\text{La}_2\text{O}_3/\text{ZnO}$, and Pd/ $\text{La}_2\text{O}_3/\text{ZnO}$ samples.

Sample	S_{BET} m^2/g	V_t cm^3/g	D_{av} nm
Pure ZnO	5.1	0.02	15
$\text{La}_2\text{O}_3/\text{ZnO}$	6.1	0.03	22
Pd/ $\text{La}_2\text{O}_3/\text{ZnO}$	5.7	0.04	27

The data show a slight increase in the specific surface area and the total pore volume for $\text{La}_2\text{O}_3/\text{ZnO}$ due to the addition of La_2O_3 and the sonication procedure, resulting in secondary porosity and new interparticle spaces. This could also be seen in the pore size distribution curves, where larger pores appear for $\text{La}_2\text{O}_3/\text{ZnO}$ and Pd/ $\text{La}_2\text{O}_3/\text{ZnO}$. The introduction of Pd does not affect the texture of the $\text{La}_2\text{O}_3/\text{ZnO}$ sample as the S_{BET} and V_t are maintained.

2.3. X-ray Diffraction

The X-ray diffraction patterns of the La-modified ZnO samples are shown in Figure 3. The main diffraction peaks of the pure ZnO sample correspond to the hexagonal wurtzite crystalline phase (PDF 01-079-2205). The La-containing phase is presented as La_2CO_5 (PDF 00-023-0320), usually formed at the first stages of La_2O_3 's reaction with air constituents (CO_2 , H_2O) [22]. After the deposition of palladium, a new phase of PdO (PDF-00-043-1024) is detected. The catalyst's phase composition remains unchanged during the catalytic test. The results of the phase composition and the mean crystallite sizes of the phases in the catalyst are presented in Table 2.

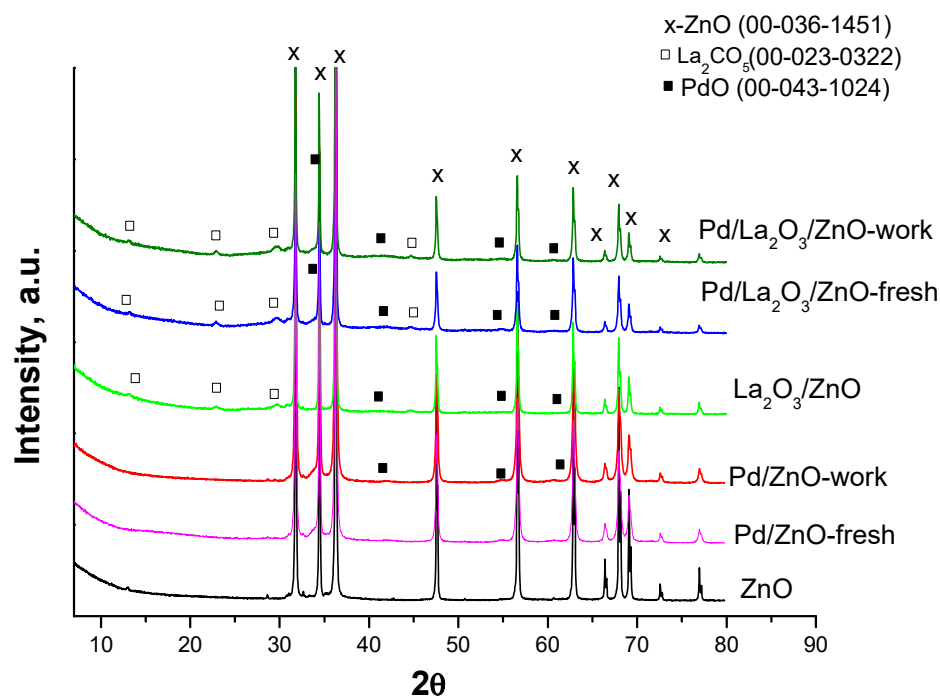


Figure 3. XRD patterns of ZnO, $\text{La}_2\text{O}_3/\text{ZnO}$, Pd/ZnO catalyst, and Pd/ $\text{La}_2\text{O}_3/\text{ZnO}$ catalyst.

Table 2. Unit cell parameters and mean crystallite sizes of the phases that are present in the catalyst.

Sample	ZnO (Parameters) Å	ZnO (Size) nm	PdO (Parameters) Å	PdO (Size) nm	La_2CO_5 (Parameters) Å	La_2CO_5 (Size) nm
ZnO	a = 3.24943(3) c = 5.20604(5)	170	-	-	-	-
PdO/ZnO—fresh	a = 3.24978(8) c = 5.2060(1)	72	a = 3.046(1) c = 5.439(2)	16	-	-
PdO/ZnO—work	a = 3.24967(7) c = 5.2058(1)	76	a = 3.046(1) c = 5.439(2)	17	-	-
$\text{La}_2\text{O}_3/\text{ZnO}$	a = 3.24966(6) c = 5.2059(1)	114	-	-	a = 4.063(5) c = 13.42(2)	5.7
Pd/ $\text{La}_2\text{O}_3/\text{ZnO}$ — fresh	a = 3.24996(10) c = 5.2060(1)	86	a = 3.040(2) c = 5.45(1)	12	a = 4.069(5) c = 13.43(3)	5.5
Pd/ $\text{La}_2\text{O}_3/\text{ZnO}$ — work	a = 3.24977(9) c = 5.2055(2)	95	a = 3.040(3) c = 5.45(1)	11	a = 4.065(5) c = 13.42(2)	5.8

It can be seen that the addition of lanthanum oxide and the sonication process [23] results in the formation of highly dispersed La_2CO_5 particles together with smaller ZnO crystallites compared to pure ZnO samples.

The influence of lanthanum oxide can also be seen after the PdO deposition stage, where a slightly higher mean crystallite size for the ZnO is observed compared to PdO deposited on pure ZnO. It is worth mentioning that the mean crystallite size of the PdO phase is lower for palladium deposited on the La₂O₃/ZnO sample. The addition of lanthanum oxide, producing small particles of La₂CO₅, also contributes the increase in the specific surface area of the catalyst.

2.4. Transmission Electron Microscopy Investigation

The TEM image of the worked Pd/La₂O₃/ZnO sample after the catalytic tests shows that the palladium-containing particles are homogeneously distributed on the surface of the catalyst (Figure 4).

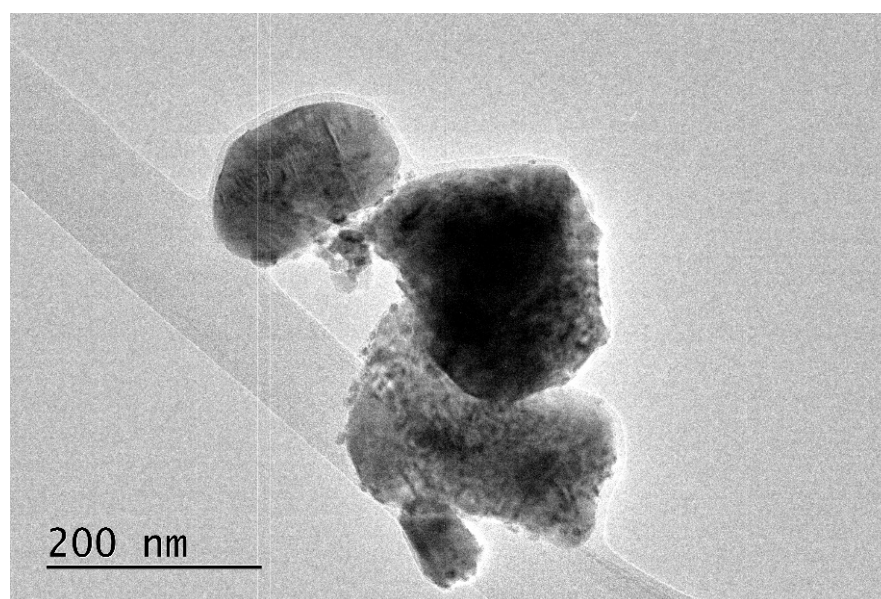


Figure 4. Bright field micrographs of Pd/La₂O₃/ZnO worked catalyst.

For the determination of the phase composition, HRTEM investigations were performed. Our observations showed that, in the fresh and worked Pd/La₂O₃/ZnO samples, palladium was presented in the form of Pd (PDF 89-4897) and tetragonal PdO (PDF 88-2434) (Figure 5).

The elemental maps (Figure 6) from the EDX analyses show the relatively homogeneous distribution of O, Zn, Pd, and La in the fresh (A) and worked (B) Pd/La₂O₃/ZnO catalysts. The results from the TEM-EDS analysis are presented in Table 3.

Table 3. TEM-EDS analyses of Pd/La₂O₃/ZnO catalyst.

Element/ Sample	O at. %	Zn at. %	Pd at. %	La at. %
Pd/La ₂ O ₃ /ZnO—fresh	42.01	57.07	0.62	0.29
Pd/La ₂ O ₃ /ZnO—work	44.38	54.58	0.94	0.10

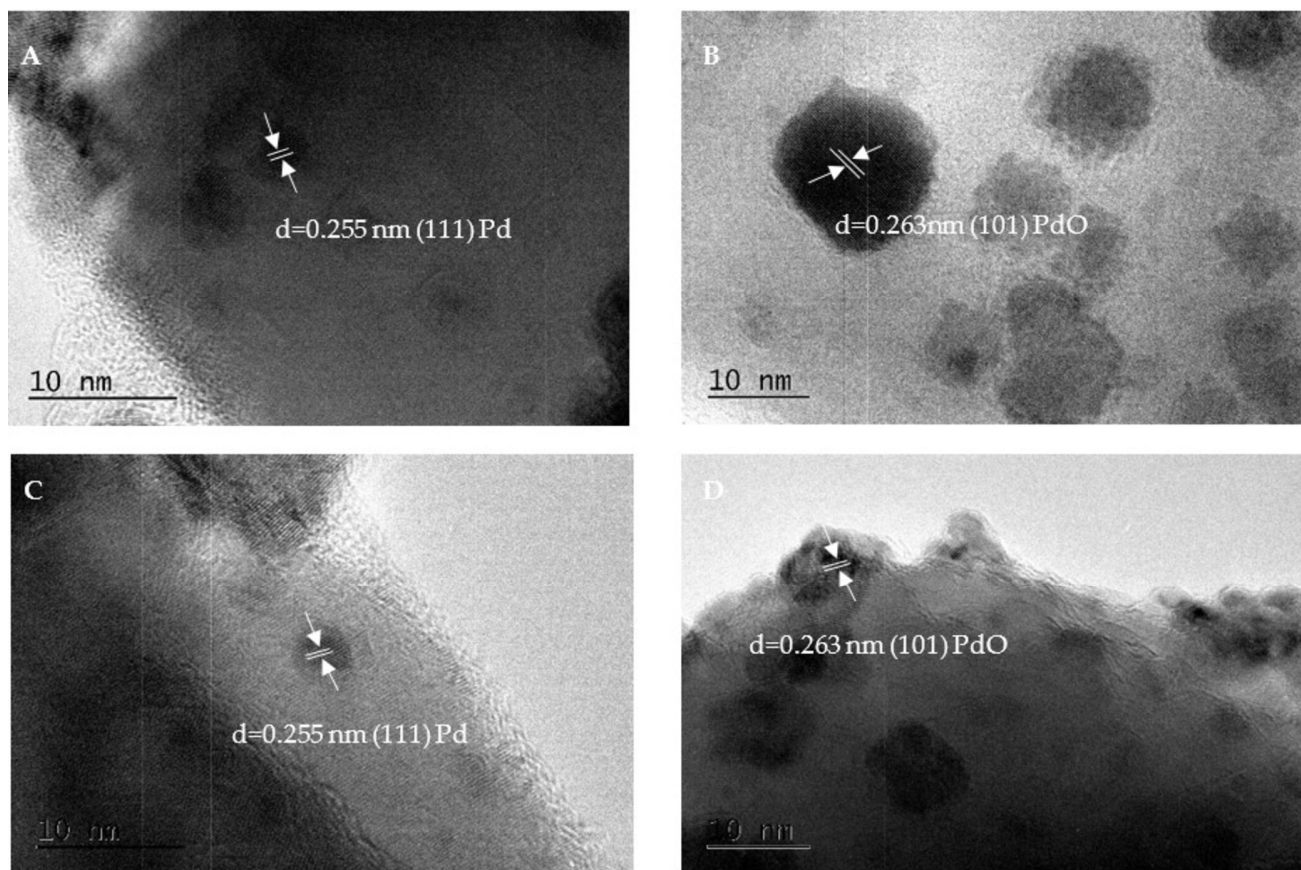


Figure 5. HRTEM images of Pd/La₂O₃/ZnO fresh sample (A,B) and Pd/La₂O₃/ZnO worked sample (C,D).

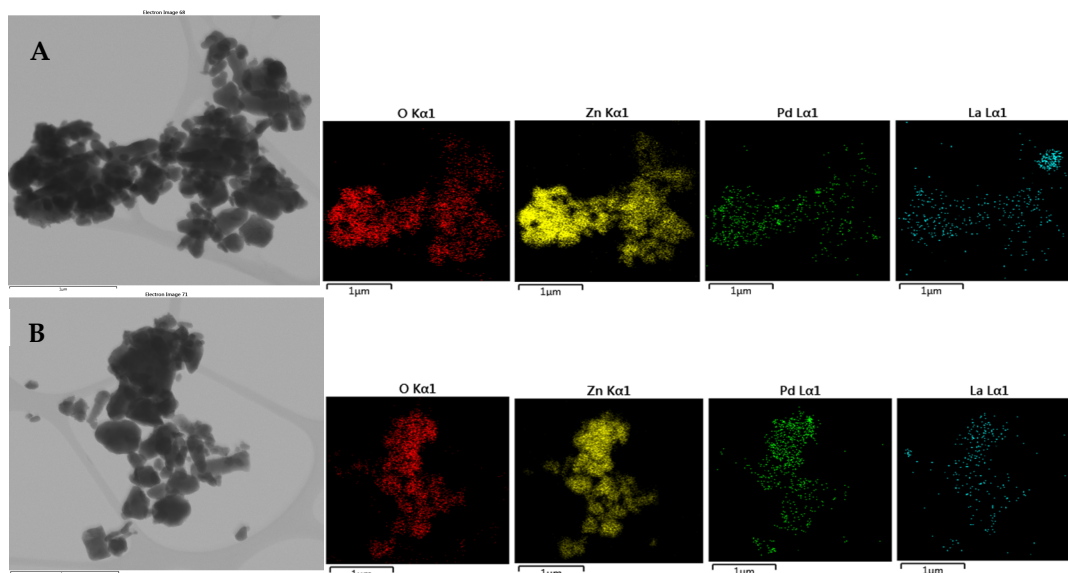


Figure 6. TEM images and O, Zn, Pd, and La elemental maps from EDX analyses of Pd/La₂O₃/ZnO fresh (A) and worked (B) catalysts.

2.5. X-ray Photoelectron Spectroscopy

Furthermore, XPS studies of the fresh and worked catalysts were carried out to obtain information on their surface compositions and chemical states. The XPS spectra of O1s, La3d, and Pd3d on the studied samples are presented in Figure 7. The XPS analysis shows that palladium is present in three different oxidation states: Pd⁰, Pd²⁺, and Pd⁴⁺

(Table 4). The formation of Pd⁴⁺ was also established in our previous studies [24,25]. As was discussed in [24], Pd⁴⁺ (PdO₂) is highly unstable, but, when the palladium particles are exposed to air for a long time, palladium oxide is formed on their surfaces, covered with a layer of PdO₂ or Pd(OH)₄.

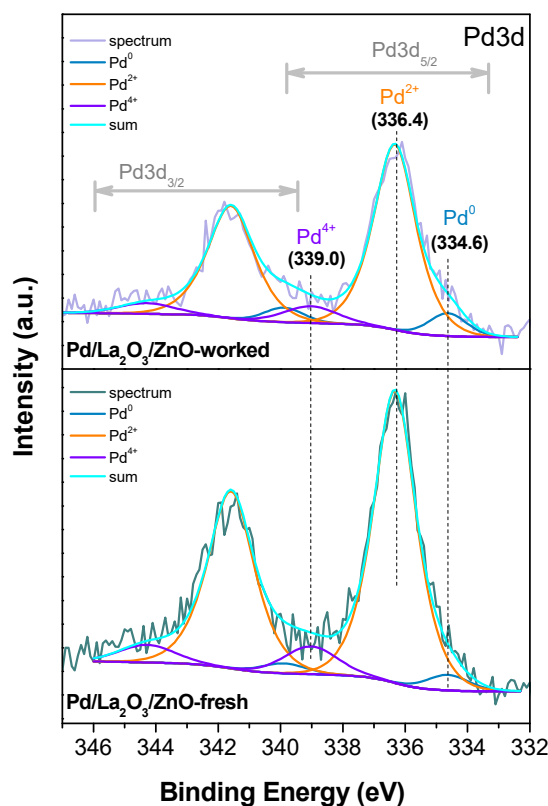


Figure 7. X-ray photoelectron spectra of Pd3d for Pd/La₂O₃/ZnO catalyst.

Table 4. Oxidation states of Pd according to XPS.

Sample	Pd ⁰ %	Pd ²⁺ %	Pd ⁴⁺ %
Pd/La ₂ O ₃ /ZnO—fresh	4.2	86.3	9.5
Pd/La ₂ O ₃ /ZnO—work	8.4	82.8	8.8

After the catalytic tests, the concentration of Pd²⁺ decreases, and the concentration of Pd⁰ increases, implying the partial reduction of Pd²⁺.

2.6. Oxygen Temperature-Programmed Desorption and Temperature-Programmed Reduction by Propane

The data obtained during the C₃H₈-TPR studies are shown in Figure 8. The heating temperature was restricted to 450 °C to collect data on the reducibility and adsorptive characteristics at such temperatures, which were comparable to those used in catalytic activity experiments. Propane was selected as a model compound for the TPR tests due to its moderate reactivity when compared with butane and methane.

The oxygen temperature-programmed desorption (O₂-TPD) results revealed that the sample could adsorb oxygen on its surface, including at room temperature (Figure 9). Increasing the temperature up to 250 °C does not result in significant O₂ desorption. Above 230 °C, the rate of O₂ desorption increases, thus revealing the higher mobility (and reactivity) of the surface oxygen in the region of the catalytic reaction. During the C₃H₈-TPR studies, the oxygen released as CO₂ should have solely originated from the

catalyst that had been exposed to propane, as the catalytic surface was considered to be “free” of adsorbed oxygen after the O₂-TPD. In the absence of gaseous oxygen, the reaction of propane oxidation on the Pd/La₂O₃/ZnO catalyst produces significantly more CO₂ than in the case of O₂ desorption. Without oxygen in the feed gas, the propane oxidation process starts at about 230 °C. With temperatures lower than 320 °C, almost all carbon from C₃H₈ is converted to CO₂. At the same temperature, the noticeable formation of CO in the C₃H₈-TPR sample is observed. When the lattice oxygen from the Pd-containing active phase is depleted, the oxidation of propane changes from complete to partial, producing CO instead of CO₂. Therefore, one may suggest the existence of two types of surface oxygen species—(i) highly mobile and reactive oxygen, connected with the Pd-containing active phase, and (ii) less reactive oxygen originating from the catalytic support.

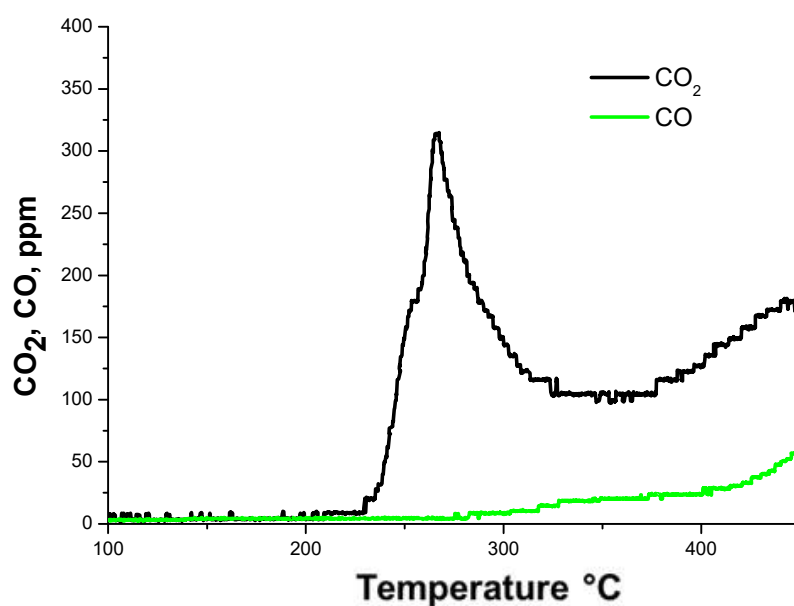


Figure 8. C₃H₈-TPR over the Pd/La₂O₃/ZnO catalyst.

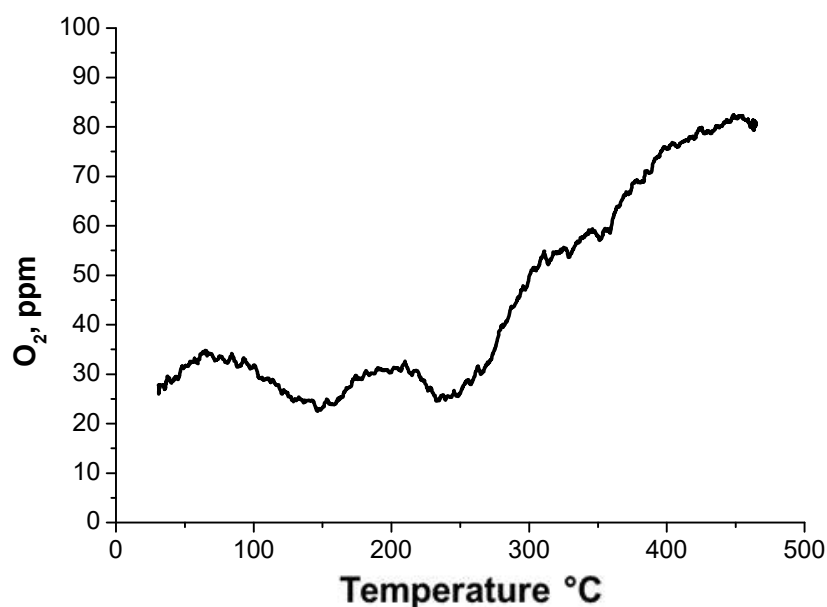


Figure 9. O₂-TPD for Pd/La₂O₃/ZnO catalyst.

2.7. Fourier Transform Infrared Spectroscopy

The formation of oxycarbonate (Figure 10) is confirmed by the three bands of νCO at 1370 cm^{-1} , 1460 cm^{-1} , and 1504 cm^{-1} (reference value: 1355 cm^{-1} , 1442 cm^{-1} , 1506 cm^{-1}) [25,26]. The shift in these bands indicates the stronger coordination of La^{3+} ions in oxycarbonate ($\text{La}_2\text{O}_3\cdot\text{CO}_2$) [25]. The formation of La_2CO_5 is confirmed by XRD. The band at 880 cm^{-1} is attributed to the δCO_3^{2-} [27]. The broad high-frequency peaks at 3420 cm^{-1} and 1631 cm^{-1} are assigned to the OH stretching of molecular-adsorbed water with hydrogen bonds or to isolated OH and to the H-O-H bending vibration of molecular water, respectively [28]. The bands at 2850 cm^{-1} , 2920 cm^{-1} , and 2964 cm^{-1} come from hydrocarbons [29–32]. The band at 493 cm^{-1} corresponds to the characteristic stretching vibrations of ZnO metal oxide bonds [33]. In the case of the pure zinc oxide sample and palladium-modified zinc oxide, two very weakly intense bands are observed at 1388 cm^{-1} and 1631 cm^{-1} . The first can be attributed to the symmetric vibration of adsorbed CO_2 [27] and the second to the H-O-H bending vibration of molecular water [28].

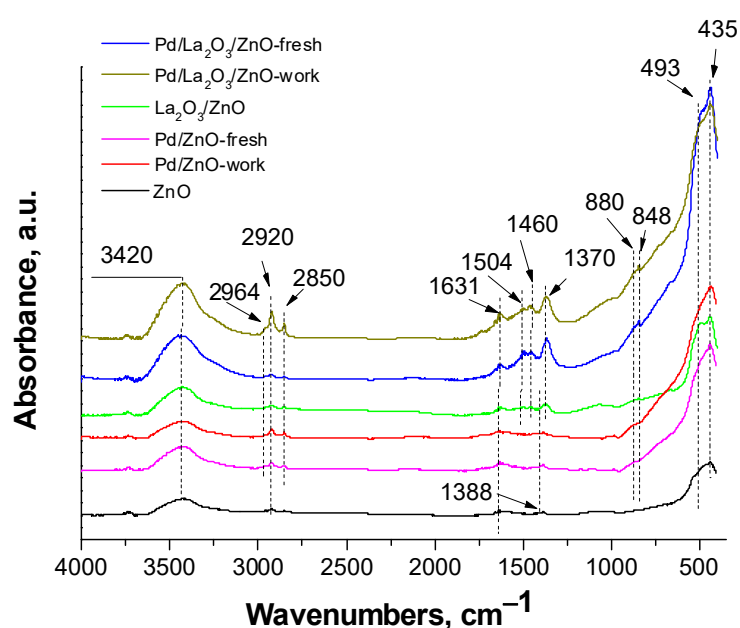


Figure 10. Infrared spectra of Pd/La₂O₃/ZnO catalyst.

It can be seen that oxycarbonates and hydrocarbons are present in the catalyst modified with lanthanum. No carbonates are formed when the support is only ZnO.

The formation of adsorbed surface compounds on the catalytically active PdO phase was not detected. As can be seen, fewer surface adsorption species are formed on the zinc oxide support; nevertheless, the catalyst with this support shows lower activity. Therefore, it can be concluded that the formation of a larger quantity of oxycarbonates and water on the surface of the Pd/La₂O₃/ZnO catalyst does not influence the catalytic activity. This is clearly seen in the catalytic activity data, showing significantly higher activity for the Pd/La₂O₃/ZnO catalyst.

3. Materials and Methods

3.1. Catalyst Sample Synthesis

Commercial ZnO powder (>99.0%), La₂O₃ (>99.0%), and absolute C₂H₅OH (Fluka, Burlington, Massachusetts) were used. Zinc oxide modified with lanthanum composite powders was produced using a simple technique, as described in [13]. A stoichiometric mixture of ZnO and La₂O₃ (2 mol.%) was prepared and mixed with ethanol. The obtained

suspension was stirred for ten minutes and sonicated for thirty minutes. The final product was obtained after one hour of drying at 100 °C. The sample was denoted as La₂O₃/ZnO.

The sample was heated for two hours at 500 °C and thus impregnated with an aqueous solution of Pd (NO₃)₂·2H₂O (99.8%, Thermo Scientific Chemicals, Waltham, MA, USA) to obtain Pd loading of 2.0 mass. %. It was further calcined for four hours at 500 °C. For comparison, a catalyst sample with 2 mass. % Pd/ZnO was prepared. The catalyst studied in this investigation was denoted as Pd/La₂O₃/ZnO.

3.2. Characterization Techniques

The texture parameters were evaluated by applying the N₂ adsorption isotherms at 77K, obtained using a Quantachrome Instruments NOVA 1200e (Quantachrome Instruments, Boynton Beach, FL, USA) instrument. The samples were outgassed at 200 °C overnight. The specific surface area was calculated by the Brunauer–Emmett–Teller (BET) equation [34]. The total pore volume was measured at a relative pressure of 0.99. The pore size distributions were obtained by the BJH [35] method, using the desorption branches of the isotherms.

Powder X-ray diffraction patterns were obtained at room temperature. The powder diffraction patterns of the fresh and spent catalysts were collected in the range of 5 to 80 degrees 2Theta on a Bruker D8 Advance diffractometer (Bruker, Karlsruhe, Germany) using Cu Kα radiation, λ = 1.5418 Å, and a LynxEye detector. Phase identification was performed with the Diffracplus EVA (V4) and ICDD-PDF2 (2021) Database. Unit cell parameters and mean crystallite sizes were determined with Topas 5.

A JEOL 2100 (JEOL Ltd., Tokyo, Japan) transmission electron microscope (TEM) operating at a 200 kV accelerating voltage was used to investigate the morphology, phase, and elemental composition. The detector was an X MAXN 80T (Oxford Instruments, Abingdon, UK). Standard holey carbon/Ni grids were dripped with suspensions that were produced by grinding and dispersing the samples in ethanol.

The electronic structure and surface composition of the catalyst were examined using X-ray photoelectron spectroscopy (XPS), employing a charge neutralization system and achromatic AlKα radiation with photon energy of 1486.6 eV, using an AXIS Supra electron-spectrometer (Kratos Analytical Ltd., Manchester, UK). Using the C1s line at 284.6 eV (adsorbed hydrocarbons), the binding energies (BE) were calculated with accuracy of ±0.1 eV. Kratos Analytical Ltd.'s commercial data-processing software ESCApe™ version 1.2.0.1325 from Kratos Analytical Ltd. was used to monitor the areas and binding energies of the C1s, O1s, La3d, and Pd3d photoelectron peaks to estimate the chemical compositions of the catalyst samples.

Oxygen temperature-programmed desorption (O₂-TPD) data were collected using a Teledyne Mod. 802 oxygen gas analyzer (paramagnetic principle). The sample was heated to 450 °C for six hours in 5% O₂ in a N₂ flow. The same gas mixture was used to cool it to room temperature. The heating rate was 10 K·min⁻¹ and the nitrogen gas flow was 500 mL·min⁻¹.

After the O₂-TPD, temperature-programmed reduction by propane (C₃H₈/TPR) tests were conducted utilizing a nitrogen gas flow (500 mL·min⁻¹) and the addition of 0.125 vol.% propane. Gas analysis for the TPR tests was carried out using an online gas analyzer with THC-FID (analyzer for total organic content in gas phase, Thermo FID-TG, SK Elektronik GmbH, Leverkusen, Germany). A multi-channel mass-flow controller system (Bronkhorst) was used to determine the compositions of the different reaction gas mixtures.

A Nicolet 6700 FTIR spectrometer (Thermo Electron Corporation, Madison, WI, USA) was used to perform Fourier transform infrared spectroscopy (FTIR). The spectral resolution was 4 cm⁻¹.

3.3. Catalytic Activity Investigation

The tests for the catalytic activity were performed in a laboratory glass reactor with continuous flow, with a 0.7 cm³ catalyst bed volume (0.5 cm³ of catalyst and 0.2 cm³ of identically sized quartz glass particles), irregularly shaped particles with an average diameter of 0.45 ± 0.15 mm, a reactor diameter of 6.0 mm, and quartz glass ($D_{\text{reactor}}/D_{\text{particles}} \geq 10$) as the experimental conditions. The fixed value of the gaseous hourly space velocity (GHSV) was 60,000 h⁻¹. The construction of the catalytic reactor permitted compensation for the adiabatic rise up to 80 °C; thus, the catalyst bed temperature was kept constant (the deviations did not exceed ±1 °C).

The pressure drop within the system was neglected. The hydrocarbon concentrations in the inlet were maintained at 0.10 vol.%, oxygen at 20.0 vol.%, and additional water vapor at 1.2 vol.%. Nitrogen (4.0) was added to all feed gas mixtures to achieve a 100% balance. The gas flow was maintained by using Bronkhorst mass-flow controllers. The water was added by an Ismatec peristaltic pump. The analysis of the reaction products was performed using a gas analyzer (MultiGas FTIR Gas Analyzer 2030G, MKS Instruments Inc., Andover, MA, USA) for CO/CO₂/O₂ determination.

4. Conclusions

A lanthanum-modified ZnO catalyst was produced using an inexpensive and easy technique. It was found that the addition of lanthanum oxide to ZnO improved the textural characteristics (specific surface area and total pore volume) of the composite support, which may have been due to the presence of small particles of La₂CO₅. These particles were formed during the sonication process, which also reduced the mean crystallite size of ZnO. The most important influence of the La additive was the decreased crystallite size of the PdO phase in the Pd/La₂O₃/ZnO sample. Three oxidation states of palladium were registered (Pd⁰, Pd²⁺, and Pd⁴⁺), and the palladium-containing phases were uniformly distributed throughout the support surface.

The catalyst Pd/La₂O₃/ZnO exhibits high catalytic activity in the complete oxidation of butane, propane, and methane, the highest being towards butane. The Pd/La₂O₃/ZnO catalyst has the potential to serve as an appropriate material in the design of eco-friendly catalysts for the elimination of waste gas pollution.

Author Contributions: Conceptualization, A.N., R.V. and N.K.; methodology, A.N., R.V. and N.K.; catalytic reactions, G.I.; XPS investigation, G.A.; XRD investigation, D.K.; N₂-physisorption, I.S.; IR investigation, S.T.; data curation, R.V.; writing—original draft preparation, A.N., R.V. and N.K.; writing—review and editing, A.N., R.V. and N.K.; visualization, R.V. All authors have read and agreed to the published version of the manuscript.

Funding: The Thermo FID-TG analyzer and MultiGas FTIR Gas Analyzer 2030G for project No. BG16RFPR002-1.014-0006, “National Center of Excellence Mechatronics and Clean Technologies”, were used for the experimental work, which was financially supported by the European Regional Development Fund under the “Research Innovation and Digitization for Smart Transformation” program 2021–2027. Research equipment for distributed research infrastructure INFRAMAT (part of the Bulgarian national roadmap for research infrastructure), supported by the Bulgarian Ministry of Education and Science, was used in this investigation.

Data Availability Statement: The original contributions presented in the study are included in the article, further inquiries can be directed to the corresponding author.

Conflicts of Interest: The authors declare no conflicts of interest.

References

1. Tokode, O.; Radhakrishna, P.; Lawton, L.A.; Robertson, P.K. Controlled periodic illumination in semiconductor photocatalysis. *J. Photochem. Photobiol. A Chem.* **2016**, *319–320*, 96–106. [\[CrossRef\]](#)
2. Bethi, B.; Shirish, H.; Sonawane, B.A.; Gumfekar, S.P. Nanomaterials-based advanced oxidation processes for wastewater treatment: A review. *Chem. Eng. Process. Process Intensif.* **2016**, *109*, 178–189. [\[CrossRef\]](#)
3. Sudha, D.; Sivakumar, P. Review on the photocatalytic activity of various composite catalysts. *Chem. Eng. Process. Process Intensif.* **2015**, *97*, 112–133. [\[CrossRef\]](#)
4. Chang, X.; Li, Z.; Zhai, X.; Sun, S.; Gu, D.; Dong, L.; Yin, Y.S.; Yanqiu, Z. Efficient synthesis of sunlight-driven ZnO-based heterogeneous photocatalysts. *Mater. Des.* **2016**, *98*, 324–332. [\[CrossRef\]](#)
5. Hemalatha, P.; Karthick, S.N.; Hemalatha, K.V.; Yi, M.; Kim, H.-J.; Alagar, M. La-doped ZnO nanoflower as photocatalyst for methylene blue dye degradation under UV irradiation. *J. Mater. Sci. Mater. Electron.* **2016**, *27*, 2367–2378. [\[CrossRef\]](#)
6. McAleer, J.F.; Moseley, P.T.; Norris, J.O.W.; Williams, D.E. Tin dioxide gas sensors. Part 1.—Aspects of the surface chemistry revealed by electrical conductance variations. *J. Chem. Soc. Faraday Trans. 1* **1987**, *83*, 1323–1346. [\[CrossRef\]](#)
7. Yamazoe, N. New approaches for improving semiconductor gas sensors. *Sens. Actuators B Chem.* **1991**, *5*, 7–19. [\[CrossRef\]](#)
8. Torres-Hernández, J.R.; Ramírez-Morales, E.; Rojas-Blanco, L.; Pantoja-Enriquez, J.; Oskam, G.; Paraguay-Delgado, F.; Escobar-Morales, B.; Acosta-Alejandro, M.; Díaz-Flores, L.L.; Pérez-Hernández, G. Structural, optical and photocatalytic properties of ZnO nanoparticles modified with Cu. *Mater. Sci. Semicond. Process.* **2015**, *37*, 87–92. [\[CrossRef\]](#)
9. Divya, N.K.; Pradyumn, P.P. Solid state synthesis of erbium doped ZnO with excellent photocatalytic activity and enhanced visible light emission. *Mater. Sci. Semicond. Process.* **2016**, *41*, 428–435. [\[CrossRef\]](#)
10. Ahmad, I.; Akhtar, M.S.; Ahmed, E.; Ahmad, M.; Keller, V.; Qamar Khan, W.; Khalid, N.R. Rare earth co-doped ZnO photocatalysts: Solution combustion synthesis and environmental applications. *Sep. Purif. Technol.* **2020**, *237*, 116328. [\[CrossRef\]](#)
11. Pandey, P.; Kurchania, R.; Haque, F.Z. Rare earth ion (La, Ce, and Eu) doped ZnO nanoparticles synthesized via sol-gel method: Application in dye sensitized solar cells. *Opt. Spectrosc.* **2015**, *119*, 666–671. [\[CrossRef\]](#)
12. Kumawat, A.; Misra, K.P.; Chattopadhyay, S. Band Gap Engineering and Relationship with Luminescence in Rare-Earth Elements Doped ZnO: An Overview. *Mat. Technol.* **2022**, *37*, 1595–1610. [\[CrossRef\]](#)
13. Kaneva, N.; Bojinova, A.; Papazova, K.; Dimitrov, D. Photocatalytic Purification of Dye Contaminated Sea Water by Lanthanide (La^{3+} , Ce^{3+} , Eu^{3+}) modified ZnO. *Catal. Today* **2015**, *252*, 113–119. [\[CrossRef\]](#)
14. Kuzhalosai, V.; Subash, B.; Shanthi, M. A novel sunshine active cerium loaded zinc oxide photocatalyst for the effective degradation of AR 27 dye. *Mater. Sci. Semicond. Process.* **2014**, *27*, 924–933. [\[CrossRef\]](#)
15. Khatamian, M.; Khandar, A.A.; Divband, B.; Haghighi, M.; Ebrahimi, S.J. Synthesis and Characterization of Dysprosium-Doped ZnO Nanoparticles for Photocatalysis of a Textile Dye under Visible Light Irradiation. *Mol. Catal. A Chem.* **2012**, *365*, 120–127. [\[CrossRef\]](#)
16. Ahmad, M.; Ahmed, E.; Zafar, F.; Khalid, N.; Niaz, N.; Hafeez, A.; Ikram, M.; Ajmal, M.; Hong, K. Enhanced photocatalytic activity of Ce-doped ZnO nanopowders synthesized by combustion method. *J. Rare Earth* **2015**, *33*, 255–262. [\[CrossRef\]](#)
17. Zboray, M.; Bell, A.T.; Iglesia, E. Role of C–H bond strength in the rate and selectivity of oxidative dehydrogenation of alkanes. *J. Phys. Chem. C* **2009**, *113*, 12380–12386. [\[CrossRef\]](#)
18. Deshlahra, P.; Iglesia, E. Reactivity and selectivity descriptors for the activation of C–H bonds in hydrocarbons and oxygenates on metal oxides. *J. Phys. Chem. C* **2016**, *120*, 16741–16760. [\[CrossRef\]](#)
19. Sharma, A.; Rani, A.; Singh, A.; Modi, O.P.; Gupta, G.K. Synthesis of alumina powder by the urea–glycine–nitrate combustion process: A mixed fuel approach to nanoscale metal oxides. *Appl. Nanosci.* **2014**, *4*, 315–323. [\[CrossRef\]](#)
20. Stefanov, P.; Todorova, S.; Naydenov, A.; Tzaneva, B.; Kolev, H.; Atanasova, G.; Stoyanova, D.; Karakirova, Y.; Alexieva, K. On the development of active and stable Pd-Co/ γ - Al_2O_3 catalyst for complete oxidation of methane. *Chem. Eng. J.* **2015**, *266*, 329–338. [\[CrossRef\]](#)
21. Velinova, R.; Todorova, S.; Drenchev, B.; Ivanov, G.; Shipochka, M.; Markov, P.; Nihtianova, D.; Kovacheva, D.; Larine, A.V.; Naydenov, A. Complex study of the activity, stability and sulphur resistance of Pd/ La_2O_3 - CeO_2 - Al_2O_3 system as monolithic catalyst for abatement of methane. *Chem. Eng. J.* **2019**, *368*, 865–876. [\[CrossRef\]](#)
22. Bernal, S.; Díaz, J.A.; García, R.; Rodríguez-Izquierdo, J.M. Study of some aspects of the reactivity of La_2O_3 with CO_2 and H_2O . *J. Mater. Sci.* **1985**, *20*, 537–541. [\[CrossRef\]](#)
23. Poli, A.L.; Batista, T.; Schmitt, C.C.; Gessner, F.; Neumann, M.G. Effect of sonication on the particle size of montmorillonite clays. *J. Coll. Interface Sci.* **2008**, *325*, 386–390. [\[CrossRef\]](#) [\[PubMed\]](#)
24. Larachi, F.; Pierre, J.; Adnot, A.; Bernis, A. Ce 3d XPS study of composite $\text{Ce}_x\text{Mn}_{1-x}\text{O}_{2-y}$ wet oxidation catalysts. *Appl. Surf. Sci.* **2002**, *195*, 236–250. [\[CrossRef\]](#)
25. Przekopa, R.E.; Marciniaka, P.; Sztorcha, B.; Czapika, A.; Stodolny, M.; Martyłac, A. One-pot synthesis of Al_2O_3 - La_2O_3 - CO_3 systems obtained from the metallic precursor by the sol-gel method. *J. Non-Cryst. Sol.* **2018**, *479*, 105–112. [\[CrossRef\]](#)

26. Pappas, G.S.; Liatsi, P.; Kartsonakis, I.A.; Danilidis, I.; Kordas, G. Synthesis and characterization of new SiO₂–CaO hollow nanospheres by sol–gel method: Bioactivity of the new system. *J. Non-Cryst. Sol.* **2008**, *354*, 755–760. [[CrossRef](#)]
27. Little, L.H. *Infrared Spectra of Adsorbed Species*; Academic Press Inc.: New York, NY, USA, 1966.
28. Gehring, A.U.; Hofmeister, A.M. The transformation of lepidocrocite during heating: A magnetic and spectroscopic study. *Clays Clay Miner.* **1994**, *42*, 409–415. [[CrossRef](#)]
29. Cornell, R.M.; Schwertmann, U. *The Iron Oxides. Structure, Properties, Reactions, Occurrences and Uses*; Wiley-VCH Verlag GmbH and Co. KGaA: Weinheim, Germany, 2003.
30. Lazaroff, N.; Sigal, W.; Wasserman, A. Iron Oxidation and Precipitation of Ferric Hydroxysulfates by Resting *Thiobacillus ferrooxidans* Cells. *Appl. Environ. Microbiol.* **1982**, *43*, 924–938. [[CrossRef](#)]
31. Music, S.; Saric, A.; Popovic, S.; Nomura, K.; Sawada, T. Forced hydrolysis of Fe³⁺ ions in NH₄Fe(SO₄)₂ solutions containing urotropin. *Croat. Chem. Acta* **2000**, *73*, 541–567. Available online: <https://hrcak.srce.hr/132070> (accessed on 5 June 2000).
32. Weckler, B.; Lutz, H.D. Lattice vibration spectra. Part XCV. Infrared spectroscopic studies on the iron oxide hydroxides goethite (α), akaganéite (β), lepidocrocite (γ), and feroxyhite (δ). *Eur. J. Solid State Inorg. Chem.* **1998**, *35*, 531–544. [[CrossRef](#)]
33. Ongun, M.Z. Tuning CO₂ sensitivity of HPTS by ZnO and ZnO@Ag nanoparticles. *J. Photochem. Photobiol. A* **2020**, *400*, 112664. [[CrossRef](#)]
34. Gomez-Serrano, V.; Gonzalez-Garcia, C.; Gonzalez-Martin, M. Nitrogen adsorption isotherms on carbonaceous materials, comparison of BET and Langmuir surface areas. *Powder Technol.* **2001**, *116*, 103–108. [[CrossRef](#)]
35. Barrett, E.P.; Joyner, L.G.; Halenda, P.P. The determination of pore volume and area distributions in porous substances. I. Computations from nitrogen isotherms. *J. Am. Chem. Soc.* **1951**, *73*, 373–380. [[CrossRef](#)]

Disclaimer/Publisher’s Note: The statements, opinions and data contained in all publications are solely those of the individual author(s) and contributor(s) and not of MDPI and/or the editor(s). MDPI and/or the editor(s) disclaim responsibility for any injury to people or property resulting from any ideas, methods, instructions or products referred to in the content.